Optical properties of $In_{1-x}Ga_xAs_yP_{1-y}$ alloys

Sadao Adachi
Department of Electronic Engineering, Faculty of Engineering, Gunma University, Kiryu-shi, Gunma 376, Japan
(Received 18 January 1989)

A method is described for the calculation of the real (ϵ_1) and imaginary (ϵ_2) parts of the dielectric function of $In_{1-x}Ga_xAs_yP_{1-y}$ quaternaries lattice matched to InP ($0 \le y \le 1.0$) at energies below and above the fundamental absorption edge. The present model is based on the Kramers-Kronig transformation and strongly connected with the electronic energy-band structure of the medium. This model reveals distinct structures at energies of the E_0, $E_0+\Delta_0$, E_1, $E_1+\Delta_1$, and E_0' (E_2) critical points (CP's). The indirect-band-gap transitions also play an important part in the spectral dependence of ϵ_2. The calculated results are in satisfactory agreement with the experimental information over the entire range of photon energies (0–6.0 eV). The compositional dependence of the optical-transition strength and broadening parameters at each CP energy and indirect band gap is also given and discussed.

I. INTRODUCTION

The (1.4–1.7)-μm spectral region is currently of great interest because of the development of low-loss silica optical fibers in this spectral region. The InGaAsP/InP quaternary alloys thus become a promising candidate for light sources and detectors used in optical-fiber communications systems.[1] These alloys are also well suited for studying the effects of alloy disorder on various phenomena, since they offer a wide range of alloy compositions ($0 \le x \le 0.48$, $0 \le y \le 1.0$) and can be obtained in a highly pure form so that the intrinsic properties should be investigated.

It is of considerable interest to investigate optical response in semiconductors.[2] Knowledge of the refractive indices and absorption coefficients of semiconductors is especially important in the design and analysis of heterostructure lasers as well as other waveguiding devices with the use of these materials.

Spectroscopic ellipsometry is an excellent technique with which to investigate the optical response of semiconductors.[3–16] Recently, Kelso *et al.*[8] have studied optical properties of $In_{1-x}Ga_xAs_yP_{1-y}$ alloys of compositions $y=0$–1.0 by spectroscopic ellipsometry. They reported room-temperature (RT) pseudodielectric-function data of $In_{1-x}Ga_xAs_yP_{1-y}$ alloys for energies from 1.5 to 6.0 eV. However, these spectral-dependence data have one disadvantage with respect to theoretical modeling: they are not expressed as continuous analytic functions of the electronic energy gaps or, also, of the alloy composition.

In this paper we present a method for calculation of the spectral dependence of the dielectric constants, $\epsilon_1(\omega)$ and $\epsilon_2(\omega)$, of $In_{1-x}Ga_xAs_yP_{1-y}$ alloys lattice matched to InP. The model is based on a simplified model of the band structure of the materials.[17–20] This model covers the optical response of semiconductors over the entire range of photon energies. In Sec. II we describe the details of our model, which includes the E_0, $E_0+\Delta_0$, E_1, $E_1+\Delta_1$, and E_0' (E_2) gaps as the main dispersion mechanisms. The effects of indirect-band-gap transitions, which will play an important part in the analysis of the ϵ_2 spectrum, are also discussed. In Sec. III we show the fits with our model to the experimental data of $In_{1-x}Ga_xAs_yP_{1-y}$ alloys reported by Kelso *et al.*[8] The compositional dependence of the strength and broadening parameters at energies of each band gap is also obtained and specified in terms of composition y alone in Sec. III. Finally, in Sec. IV the conclusions obtained in this study are briefly summarized.

II. THEORETICAL EXPRESSION

The joint-density-of-states functions $J_{cv}(\omega)$ can be related to the optical constant $\epsilon_2(\omega)$:

$$\epsilon_2(\omega)=\frac{4\hbar^2e^2}{\pi m^2\omega^2}|\langle c|p|v\rangle|^2 J_{cv}(\omega) , \tag{1}$$

where $\langle |p| \rangle$ is the momentum matrix element for v (valence)$\rightarrow c$ (conduction) transitions. Real (ϵ_1) and imaginary parts (ϵ_2) of the dielectric function are also connected by the Kramers-Kronig (KK) relations:

$$\epsilon_2(\omega)=-\frac{2}{\pi}\int_0^\infty \frac{\epsilon_1(\omega')}{(\omega')^2-\omega^2}d\omega' , \tag{2a}$$

$$\epsilon_1(\omega)=1+\frac{2}{\pi}\int_0^\infty \frac{\omega'\epsilon_2(\omega')}{(\omega')^2-\omega^2}d\omega' . \tag{2b}$$

In the following we will summarize the model dielectric functions for the critical points (CP's) of various transition energies [E_0, $E_0+\Delta_0$, E_1, $E_1+\Delta_1$, and E_0' (E_2)].[17–20] The effects of indirect-band-gap transitions, which will play an important part in the analysis of the ϵ_2 spectrum, are also discussed briefly.

A. E_0 and $E_0+\Delta_0$ transitions

The E_0 and $E_0+\Delta_0$ transitions in the diamond- and zinc-blende-type semiconductors occur in the center of

the Brillouin zone (BZ). These transitions are of the three-dimensional (3D) M_0 CP's. The compositional dependence of E_0 and $E_0+\Delta_0$ in the $In_{1-x}Ga_xAs_yP_{1-y}$ quaternary system is expressed by the following quadratic form with respect to the molar composition y:[21,22]

$$E_0(y)=1.35-0.72y+0.12y^2 , \tag{3}$$

$$E_0+\Delta_0(y)=1.466-0.557y+0.129y^2 . \tag{4}$$

Assuming the bands are parabolic, and using the KK relations, we obtain the contribution of these band gaps to $\epsilon_2(\omega)$ and $\epsilon_1(\omega)$:

$$\epsilon_2(\omega)=[A/(\hbar\omega)^2][(\hbar\omega-E_0)^{0.5}H(x_0-1)+\tfrac{1}{2}(\hbar\omega-E_0-\Delta_0)^{0.5}H(\chi_{\text{s.o.}}-1)] , \tag{5}$$

$$\epsilon_1(\omega)=AE_0^{-1.5}\{f(\chi_0)+\tfrac{1}{2}[E_0/(E_0+\Delta_0)]^{1.5}f(\chi_{\text{s.o.}})\} , \tag{6}$$

with

$$A=\tfrac{4}{3}(\tfrac{3}{2}m^*)^{1.5}P^2 , \tag{7}$$

$$f(\chi_0)=\chi_0^{-2}[2-(1+\chi_0)^{0.5}-(1-\chi_0)^{0.5}H(1-\chi_0)] , \tag{8a}$$

$$f(\chi_{\text{s.o.}})=\chi_{\text{s.o.}}^{-2}[2-(1+\chi_{\text{s.o.}})^{0.5}-(1-\chi_{\text{s.o.}})^{0.5}H(1-\chi_{\text{s.o.}})] , \tag{8b}$$

$$\chi_0=\hbar\omega/E_0 , \tag{9a}$$

$$\chi_{\text{s.o.}}=\hbar\omega/(E_0+\Delta_0) , \tag{9b}$$

and

$$H(z)=\begin{cases}1 & \text{for } z\geq 0\\ 0 & \text{for } z<0 .\end{cases} \tag{10}$$

In Eq. (7), m^* is the combined density-of-states mass and P^2 is the squared momentum matrix element.

As we will see later, the strength of the E_0 and $E_0+\Delta_0$ transitions in the $In_{1-x}Ga_xAs_yP_{1-y}$ quaternary system is very weak. This is due to the small density of states associated with these transitions (i.e., due to the small effective mass of the Γ_6 conduction band).

B. E_1 and $E_1+\Delta_1$ transitions

The E_1 and $E_1+\Delta_1$ transitions in the $In_{1-x}Ga_xAs_yP_{1-y}$ quaternary system may take place along the $\langle 111\rangle$ directions (Λ) or at L points in the BZ. The variation with composition of these transition energies can be written as[8]

$$E_1(y)=3.163-0.590y+0.33y^2 , \tag{11}$$

$$E_1+\Delta_1(y)=3.296-0.466y+0.26y^2 . \tag{12}$$

The E_1 and $E_1+\Delta_1$ CP's are of the 3D M_1 type. The contributions to ϵ_2 of this type are

$$\epsilon_2(\omega)=\begin{cases}\pi\chi_1^{-2}[B_1-B_{11}(E_1-\hbar\omega)^{0.5}] & (\hbar\omega<E_1) ,\\ \pi B_1\chi_1^{-2} & (\hbar\omega\geq E_1) ,\end{cases} \tag{13}$$

for the E_1 transitions, and

$$\epsilon_2(\omega)=\begin{cases}\pi\chi_{1s}^{-2}[B_2-B_{21}(E_1+\Delta_1-\hbar\omega)^{0.5}] & (\hbar\omega<E_1+\Delta_1) ,\\ \pi B_2\chi_{1s}^{-2} & (\hbar\omega\geq E_1+\Delta_1) ,\end{cases} \tag{14}$$

for the $E_1+\Delta_1$ transitions, where

$$\chi_1=\hbar\omega/E_1 , \tag{15}$$

$$\chi_{1s}=\hbar\omega/(E_1+\Delta_1) . \tag{16}$$

In Eqs. (13) and (14), the B's are the strength parameters. Since the M_1 CP longitudinal effective mass is much larger than its transverse counterparts, one can treat these 3D M_1 CP's as two-dimensional (2D) minima M_0. The contribution to ϵ_2 of this type of 2D minima is given by

$$\epsilon_2(\omega)=\pi[B_1\chi_1^{-2}H(\chi_1-1)+B_2\chi_{1s}^{-2}H(\chi_{1s}-1)] , \tag{17}$$

where the H's are functions defined by Eq. (10).

The KK transformation of Eq. (17) gives

$$\epsilon_1(\omega)=-B_1\chi_1^{-2}\ln(1-\chi_1^2)-B_2\chi_{1s}^{-2}\ln(1-\chi_{1s}^2) . \tag{18}$$

The first and second terms on the right-hand side of Eq. (18), respectively, correspond to the E_1 and $E_1+\Delta_1$ gap contributions.

C. E_0' (E_2) transitions

The more pronounced structure found in the $In_{1-x}Ga_xAs_yP_{1-y}$ system in the region higher in energy than E_1 is labeled E_0' (E_0' triplet). The E_0' transitions in the zinc-blende-type semiconductors are believed to take place at the Γ point, or in the Δ direction near the Γ point. The spin-orbit interaction splits the single-group Γ_{15}^c conduction band into the double-group Γ_7^c and Γ_8^c bands (splitting energy Δ_0'), and the single-group Γ_{15}^v valence band into the double-group Γ_8^v and Γ_7^v bands (splitting energy Δ_0). The corresponding transitions at $\mathbf{k}=0$ (Γ) are, respectively, labeled E_0' ($\Gamma_8^v\rightarrow\Gamma_7^c$), $E_0'+\Delta_0'$ ($\Gamma_8^v\rightarrow\Gamma_8^c$), $E_0'+\Delta_0$ ($\Gamma_7^v\rightarrow\Gamma_7^c$; dipole forbidden), and $E_0'+\Delta_0'$ ($\Gamma_7^v\rightarrow\Gamma_8^c$).

The band-structure calculation of Chelikowsky and Cohen[23] for InP suggests various CP's in this energy region. Three of them correspond to transitions at the Γ point (i.e., E_0', $E_0'+\Delta_0'$, and $E_0'+\Delta_0'+\Delta_0$). The $E_0'+\Delta_0'+\Delta_0$ transitions are thought to be too weak to be dominant in optical spectra. A further transition, found in the calculation, is located along [100] (Δ) about 20% of the way to X [$E_0'(\Delta);\Delta_5^v\rightarrow\Delta_5^c$]. The E_2 transitions are also expected to take place along the [110] direction (Σ) or near X, and occur in InP for energies close to the E_0' and $E_0'+\Delta_0'$ CP's. However, the strength of the E_2 transitions in InP seems to be much weaker than the strength

of the E_0' and $E_0'+\Delta_0'$ transitions. In an earlier work,[24] the $E_0'+\Delta_0'$ transitions in InP were attributed to E_2 CP's. However, from theoretical considerations about the spin-orbit splitting of the conduction band (Δ_0'), the structure has more recently been assigned to the $E_0'+\Delta_0'$ transitions.[8] For compositions $y\neq 0$, the structure has also never been resolved for more than two of the three most prominent expected features (E_0', $E_0'+\Delta_0'$, and E_2). It has thus been considered that this is due to overlapping or "missing" structures (i.e., due to their weak structures).

The E_0' and $E_0'+\Delta_0'$ transitions in the $In_{1-x}Ga_xAs_yP_{1-y}$ system cannot be clearly resolved in the rather broad CP's observed ellipsometrically (i.e., ϵ_1 and ϵ_2).[8] Therefore, we consider only the E_0' CP's as the main dispersion source in this spectral region. The variation with composition of this transition energy can be written as[8]

$$E_0'(y)=4.72-0.31y-0.01y^2 . \tag{19}$$

If the E_0' transitions occur at Γ (Δ), then the CP should be of the 3D M_0 (3D M_1) type.[8] However, it is found from the present analyses that neither the 3D M_0 nor the 3D M_1 model represents the peculiar line shapes of ϵ_1 and ϵ_2 in the E_0' spectral region. The best fits are obtained with a damped-harmonic-oscillator (DHO) model, as in the case of the E_2 CP's for some III-V binaries (such as GaP, GaSb, and InAs) (Ref. 17), $Al_xGa_{1-x}As$ (Ref. 18), Si (Ref. 19), Ge (Ref. 19), and α-Sn (Ref. 20).

The DHO gives

$$\epsilon_2(\omega)=C\chi_2\gamma/[(1-\chi_2^2)^2+\chi_2^2\gamma^2] , \tag{20}$$

$$\epsilon_1(\omega)=C(1-\chi_2^2)/[(1-\chi_2^2)^2+\chi_2^2\gamma^2] , \tag{21}$$

with

$$\chi_2=\hbar\omega/E_0' , \tag{22}$$

where C and γ are, respectively, the strength and broadening parameters of the oscillator.

D. Indirect-band-gap transitions

Even though the basic $In_{1-x}Ga_xAs_yP_{1-y}$/InP heterostructure concepts are understood at this time, some practical device parameters in this system have been hampered by a lack of definite knowledge of many material parameters. To our knowledge, no detailed information is available about the indirect-band-gap energy E_g^{id} in this alloy system. This necessitates the use of some sort of an interpolation scheme.[25–27] Let us now estimate the indirect-band-gap energies E_g^X ($\Gamma_8^v\rightarrow X_6^c$) and E_g^L ($\Gamma_8^v\rightarrow L_6^c$) over the entire range of alloy composition for $In_{1-x}Ga_xAs_yP_{1-y}$ lattice matched to InP.

The quaternary alloy, $In_{1-x}Ga_xAs_yP_{1-y}$, is thought to be constructed of four ternary compounds: $In_{1-x}Ga_xP$, $In_{1-x}Ga_xAs$, $GaAs_yP_{1-y}$, and $InAs_yP_{1-y}$. The material parameters in many ternary alloys (e.g., $A_xB_{1-x}C$) can be usually approximated in the form of a quadratic function: $T_{ABC}(x)=xB_{AC}+(1-x)B_{BC}+x(x-1)c$,[28] where the B's are material parameters of the corresponding binaries (AC and BC) and c is referred to as a bowing parameter for the ternary material ABC. If relationships for the ternary material parameters (T's) are available, the quaternary parameter $Q(x,y)$ can be given by

$$Q(x,y)=\frac{1}{x(1-x)+y(1-y)}\{x(1-x)[yT_{ABC}(x)+(1-y)T_{ABD}(x)]+y(1-y)[xT_{ACD}(y)+(1-x)T_{BCD}(y)]\} . \tag{23}$$

In Table I we present the indirect-band-gap energies E_g^X and E_g^L for the binaries of interest. Table II also lists the bowing parameters of the indirect-band-gap energies E_g^X and E_g^L for some ternaries of interest.

Among various material parameters, the lattice constant is known to obey Vegard's law well, i.e., to vary linearly with alloy composition. Using this law, the lattice-matching relation between the compositions x and y for $In_{1-x}Ga_xAs_yP_{1-y}$ to InP is written as[29]

$$x=\frac{0.1896y}{0.4176-0.0125y} . \tag{24}$$

The quaternary indirect-band-gap energies as a function of composition are obtained by numerical solution of Eq. (23), using the relation of Eq. (24) and numerical values listed in Tables I and II. In Fig. 1 we present the indirect-band-gap energies E_g^X and E_g^L as a function of the y-composition parameter for $In_{1-x}Ga_xAs_yP_{1-y}$ lattice matched to InP. The variation with composition of the E_0 [Eq. (3)], $E_0+\Delta_0$ [Eq. (4)], E_1 [Eq. (11)], $E_1+\Delta_1$ [Eq. (12)], and E_0' (E_2) gaps [Eq. (19)] is also plotted in the figure. It is evident from the figure that the quaternary system has a direct band gap [$E_0/(E_0+\Delta_0)$] as the

TABLE I. Indirect-band-gap energies of some III-V binary compounds (RT).

Binary	E_g^X (eV)	E_g^L (eV)
GaP	2.26	2.63
GaAs	1.91	1.73
InP	2.21	2.05
InAs	1.37	1.07

TABLE II. Indirect-band-gap bowing parameters of some III-V ternary compounds (RT).

Ternary	Bowing parameter (eV) E_g^X	E_g^L
$In_{1-x}Ga_xP$	0.18	0.43
$In_{1-x}Ga_xAs$	1.4	0.72
$GaAs_yP_{1-y}$	0.21	0.42
$InAs_yP_{1-y}$	0.28	0.27

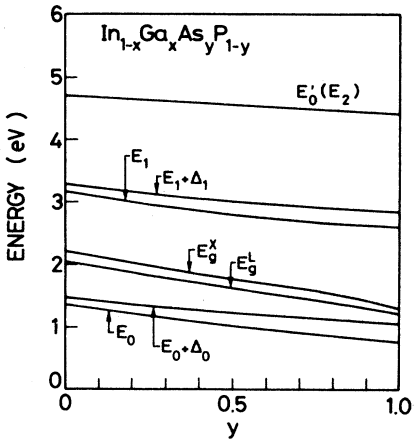

FIG. 1. Variation with composition y of E_0, $E_0+\Delta_0$, E_1, $E_1+\Delta_1$, $E_0'(E_2)$, E_g^X, and E_g^L (see text).

fundamental absorption edge in a full range of the y composition ($0 \le y \le 1.0$). It is also found that the indirect band gaps E_g^X and E_g^L lie in energies between the $E_0/(E_0+\Delta_0)$ and $E_1/(E_1+\Delta_1)$ gaps. Thus, the indirect-band-gap transitions (E_g^X and E_g^L) occur after the onset of the $E_0/(E_0+\Delta_0)$ direct-band-gap transitions but before the predominance of the $E_1/(E_1+\Delta_1)$ direct-band-gap transitions. It is also worth noting that the E_g^X gap lies above the E_g^L one. This leads to a prediction of the Γ_6-L_6-X_6 conduction-band order of increasing energy assured in a full composition range of this quaternary system. In the present analysis, we shall consider only the lowest indirect band gap E_g^L as the dispersion source in the indirect-band-gap optical response.

The optical-transition mechanism at the indirect band gap, $E_g^{\rm id}$, is expressed usually by a second-order process in the perturbation. Using the result of the second-order time-dependent perturbation calculation, we can write the contribution of the indirect optical transitions to ϵ_2 as

$$\epsilon_2(\omega)=\frac{D}{(\hbar\omega)^2}(\hbar\omega-E_g^{\rm id}+\hbar\omega_q)^2 H(1-\chi_g)\ , \tag{25}$$

with

$$\chi_g=(E_g^{\rm id}-\hbar\omega_q)/\hbar\omega\ , \tag{26}$$

where D is the indirect-transition strength parameter, and $\hbar\omega_q$ is the phonon energy taking part in the indirect transitions. In Eq. (25), only the phonon-absorption process is taken into account. The phonon-emission process remains possible, however, because the only difference from the above case is the sign of the phonon energy.

The parabolic bands extending to infinite energies implied by Eq. (25) should be nonphysical. We shall, therefore, modify the model by taking into account a high-energy cutoff at the energy E_c. This modification gives

$$\epsilon_2(\omega)=\frac{D}{(\hbar\omega)^2}(\hbar\omega-E_g^{\rm id}+\hbar\omega_q)^2 H(1-\chi_g)H(1-\chi_c) \tag{27}$$

with

$$\chi_c=\hbar\omega/E_c\ . \tag{28}$$

The cutoff energy E_c is assumed in the present analyses to be the same value as E_1 (i.e., $E_c=E_1$).

Unfortunately, there has been no expression for the contribution of the indirect transitions to ϵ_1. Analytical expressions for this contribution from the KK transformation are also not yet available. We will, therefore, take into account the contribution of the indirect transitions only to ϵ_2, but not to ϵ_1.

III. RESULTS AND DISCUSSION

A. A comparison of our model to experimental spectra

The model given in Sec. II can be used to fit the experimental dispersion of ϵ_2 and ϵ_1 over most of the spectral range (0–6.0 eV). The parameters, such as A, B_1, and C, can be commonly used as adjustable constants for the calculation of both ϵ_2 and ϵ_1. The experimental data of ϵ_1 in the transparent region are, however, usually somewhat larger than those of our model [i.e., the sum of Eqs. (6), (18), and (21)]. In order to improve a fit, therefore, we shall consider an additional term, $\epsilon_{1\infty}$, to ϵ_1. This term is assumed to be nondispersive (i.e., constant) and may arise from the indirect-band-gap and other higher-lying, band-gap transitions (E_1', $E_1'+\Delta_1'$, $E_2+\Delta_2$, etc.).

The fits with our model to the experimental ϵ_2 and ϵ_1 of InP ($x=0$, $y=0$) are shown in Figs. 2 and 3, respectively. In Fig. 2 the solid line is obtained from the sum of Eqs. (5), (13), (14), (20), and (27). The dashed line is the result of the sum of Eqs. (5), (17), and (20). The numerical parameters of the fits are listed in Table III. The experimental data are taken below 1.7 eV from Ref. 30 (open circles) and above 1.5 eV from Ref. 8 (solid circles).

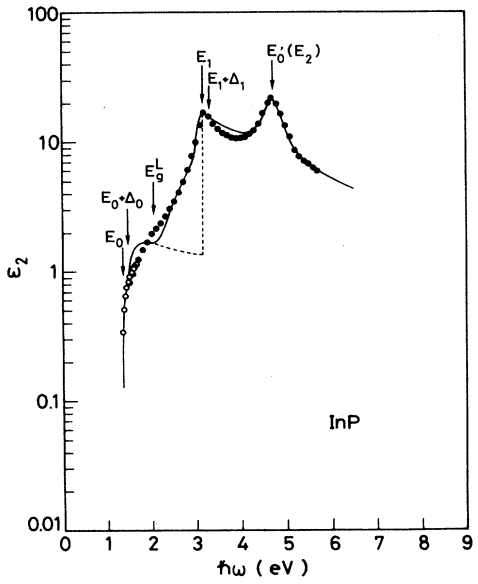

FIG. 2. ϵ_2 spectrum of InP ($x=0$, $y=0$). The solid line is obtained from the sum of Eqs. (5), (13), (14), (20), and (27). The dashed line is the result of the sum of Eqs. (5), (17), and (20). The experimental data are taken below 1.7 eV from Ref. 30 (open circles) and above 1.5 eV from Ref. 8 (solid circles).

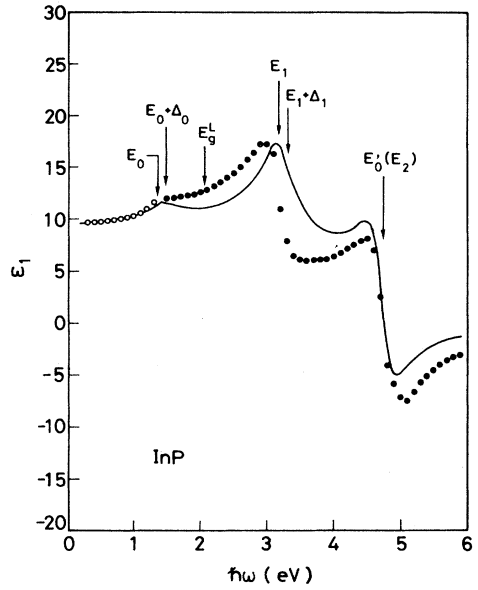

FIG. 3. ϵ_1 spectrum of InP ($x=0$, $y=0$). The solid line is obtained from the sum of Eqs. (6), (18) ($\Gamma=0.14$ eV), and (21). The nondispersive term, $\epsilon_{1\infty}$ (=2.1), is taken into consideration in this calculation. The experimental data (solid circles) are taken from Ref. 8. The data in the transparency region (open circles) are taken from our previous calculation (Ref. 25).

As discussed in Sec. II, we are able to fit the E_1 (and $E_1+\Delta_1$) CP structure with either the 2D [Eq. (17)] or 3D model [Eqs. (13) and (14)]. The 3D model explains the experimental lower-energy shoulder of this structure well. The fit in the (2–3)-eV region also becomes satisfactory when the indirect-band-gap contribution [Eq. (27)] is taken into account. The E_0' (E_2) structure is seen to be well fitted by the DHO [Eq. (20)].

In Fig. 3 the solid line is obtained from the sum of Eqs. (6), (18), and (21). The nondispersive term, $\epsilon_{1\infty}$ (=2.1), is taken into consideration in this calculation. The experimental data (solid circles) are taken from Ref. 8. The data in the transparency region (open circles) are taken from our previous calculation (Ref. 25). As discussed in Refs. 17–20 (also see Fig. 9), the theoretical ϵ_1 spectrum [Eq. (18)] exhibits a divergence at the E_1 and $E_1+\Delta_1$ edges. An introduction of the damping (broadening) effect into Eq. (18) can successfully decrease the strength of the E_1 and $E_1+\Delta_1$ peaks and lead to a fact which is coincident with experimental verification. Such a damping effect can be easily introduced in Eq. (18) in a phenomenological manner by replacing ω by $\omega+i(\Gamma/\hbar)$. The best-fit value of Γ obtained is 0.14 eV. It is also seen in the figure that a dramatic change in ϵ_1 near the 4.5-eV region can be well explained by the DHO model of the E_0' (E_2) structure [Eq. (21)].

Figures 4 and 5 show, respectively, the fits with our model to the experimental ϵ_2 and ϵ_1 spectra of $In_{1-x}Ga_xAs_yP_{1-y}$ ($x=0.25$, $y=0.55$). In Fig. 4, the solid line is obtained from the sum of Eqs. (5), (13), (14), (20), and (27). The dashed line is the result of the sum of Eqs. (5), (17), and (20). The experimental data (solid circles) are taken from Ref. 8. In Fig. 5 the solid line is obtained from the sum of Eqs. (6), (18) ($\Gamma=0.11$ eV), and (21). The nondispersive term, $\epsilon_{1\infty}$ (=2.1), is taken into consideration in this calculation. The solid and open circles are, respectively, taken from Refs. 8 and 25. As in the case of InP, we see in the figures better fits with our model to the experimental data over the entire range of photon energies.

The fits with our model to the experimental ϵ_2 and ϵ_1 spectra of $In_{1-x}Ga_xAs$ ($x=0.48$, $y=1.0$) are shown in Figs. 6 and 7, respectively. In Fig. 6 the solid line is the result of the sum of Eqs. (5), (13), (14), (20), and (27). The dashed line is obtained from the sum of Eqs. (5), (17), and (20). The experimental data are taken below 1.0 eV from Ref. 30 (open circles) and above 1.5 eV from Ref. 8 (solid circles). It is clear that the indirect-band-gap [Eq. (27)] and 3D saddle-point terms [Eqs. (13) and (14)] interpret well the (1.5–3.0)-eV region of the ϵ_2 spectrum. In Fig. 7, the solid line is the result of the sum of Eqs. (6), (18), and (21). The nondispersive term, $\epsilon_{1\infty}$ (=2.8), is taken into

TABLE III. Parameters used in the calculation of $\epsilon_2(\omega)$ and $\epsilon_1(\omega)$.

Parameter	Composition y 0	0.24	0.42	0.55	0.82	1.00
E_0 (eV)	1.35	1.18	1.07	0.99	0.84	0.75
$E_0+\Delta_0$ (eV)	1.47	1.34	1.25	1.20	1.10	1.04
E_1 (eV)	3.16	2.96	2.83	2.76	2.63	2.57
$E_1+\Delta_1$ (eV)	3.30	3.14	3.04	2.98	2.88	2.83
E_0' (eV)	4.72	4.65	4.59	4.55	4.47	4.41
E_g^L (eV)	2.05	1.83	1.68	1.58	1.38	1.20
A ($eV^{1.5}$)	5.40	4.39	3.64	3.09	1.96	1.20
B_1	4.91	4.30	3.69	3.71	3.78	3.84
B_2	0.09	0.53	1.04	1.06	1.37	1.48
B_{11} ($eV^{-0.5}$)	10.32	8.76	7.28	7.53	7.91	7.57
B_{21} ($eV^{-0.5}$)	0.18	1.06	2.08	2.12	2.74	2.96
Γ (eV)	0.14	0.12	0.12	0.11	0.13	0.14
C	1.30	1.98	2.49	2.77	3.10	2.90
γ	0.093	0.145	0.183	0.204	0.239	0.225
D	60.4	39.0	30.4	29.4	24.0	20.7
$\epsilon_{1\infty}$	2.1	2.1	2.1	2.1	2.1	2.8

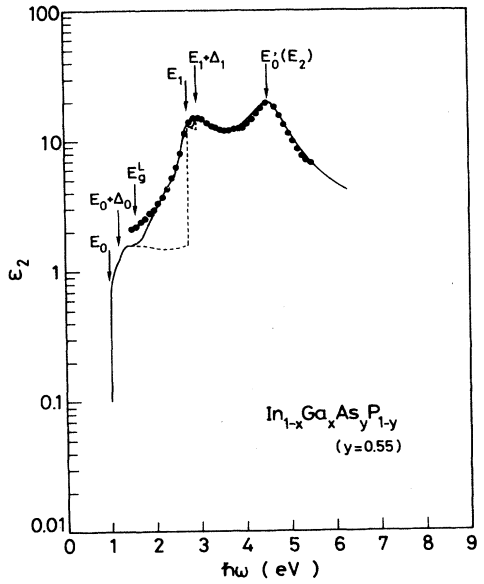

FIG. 4. ϵ_2 spectrum of $In_{1-x}Ga_xAs_yP_{1-y}$ ($x=0.25$, $y=0.55$). The solid line is obtained from the sum of Eqs. (5), (13), (14), (20), and (27). The dashed line is the result of the sum of Eqs. (5), (17), and (20). The experimental data (solid circles) are taken from Ref. 8.

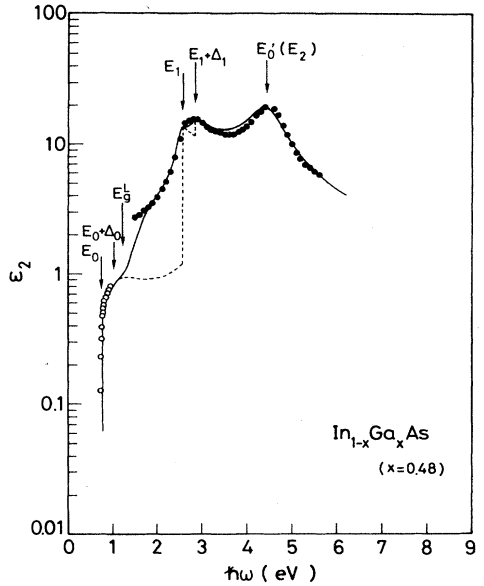

FIG. 6. ϵ_2 spectrum of $In_{1-x}Ga_xAs$ ($x=0.48$, $y=1.0$). The solid line is the result of the sum of Eqs. (5), (13), (14), (20), and (27). The dashed line is obtained from the sum of Eqs. (5), (17), and (20). The experimental data are taken below 1.0 eV from Ref. 30 (open circles) and above 1.5 eV from Ref. 8 (solid circles).

consideration in this calculation. The solid and open circles are, respectively, taken from Refs. 8 and 25. The experimental value of ϵ_1 at the E_1 peak is about 19. The smaller the damping energy Γ, the larger the E_1 peak value.[17] The calculation with $\Gamma=0.14$ eV agrees well with this value.

An individual contribution to ϵ_2 of the $E_0/(E_0+\Delta_0)$, $E_1/(E_1+\Delta_1)$, E_0' (E_2), and E_g^L gap for $In_{1-x}Ga_xAs_yP_{1-y}$ ($x=0.25$, $y=0.55$) is shown in Fig. 8. They are obtained from Eq. (5) (3D M_0) for the $E_0/(E_0+\Delta_0)$ gap contribution, from Eqs. (13) and (14) (3D M_1, solid lines) and Eq. (17) (2D M_0, dashed lines)

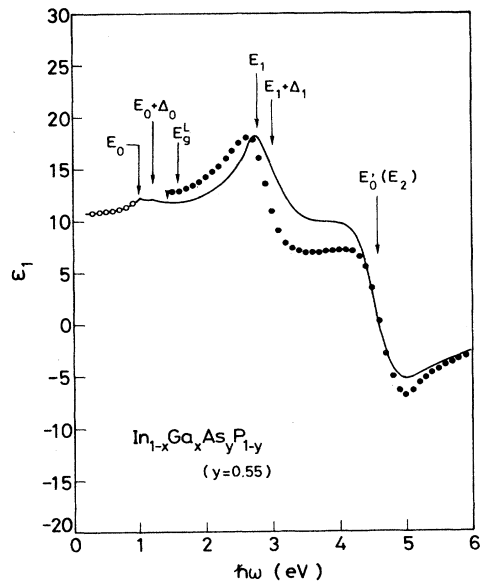

FIG. 5. ϵ_1 spectrum of $In_{1-x}Ga_xAs_yP_{1-y}$ ($x=0.25$, $y=0.55$). The solid line is obtained from the sum of Eqs. (6), (18) ($\Gamma=0.11$ eV), and (21). The nondispersive term, $\epsilon_{1\infty}$ ($=2.1$), is taken into consideration in this calculation. The solid and open circles are, respectively, taken from Refs. 8 and 25.

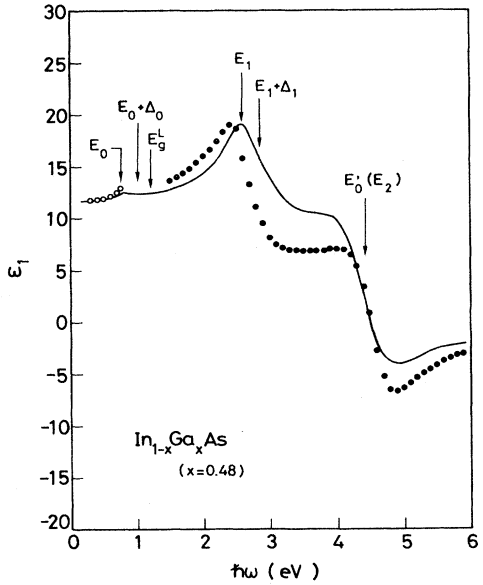

FIG. 7. ϵ_1 spectrum of $In_{1-x}Ga_xAs$ ($x=0.48$, $y=1.0$). The solid line is the result of the sum of Eqs. (6), (18) ($\Gamma=0.14$ eV), and (21). The nondispersive term, $\epsilon_{1\infty}$ ($=2.8$), is taken into consideration in this calculation. The solid and open circles are, respectively, taken from Refs. 8 and 25.

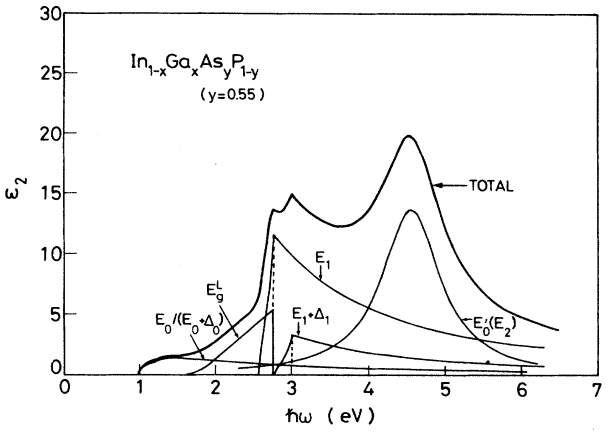

FIG. 8. Individual contribution to ϵ_2 of the $E_0/(E_0+\Delta_0)$, $E_1/(E_1+\Delta_1)$, E_0' (E_2), and E_g^L gaps for $In_{1-x}Ga_xAs_yP_{1-y}$ $(x=0.25,\ y=0.55)$. They are obtained from Eq. (5) (3D M_0) for the $E_0/(E_0+\Delta_0)$ gap contribution, from Eqs. (13) and (14) (3D M_1, solid lines), and Eq. (17) (2D M_0, dashed lines) for the $E_1/(E_1+\Delta_1)$ gap contribution, from Eq. (20) (DHO) for the E_0' (E_2) gap contribution, and from Eq. (27) for the E_g^L gap contribution. The sum of these contributions is shown by the bold line.

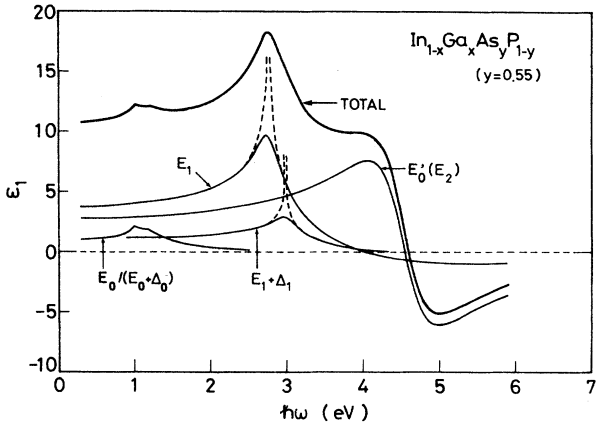

FIG. 9. Individual contribution to ϵ_1 of the $E_0/(E_0+\Delta_0)$, $E_1/(E_1+\Delta_1)$, and E_0' (E_2) transitions for $In_{1-x}Ga_xAs_yP_{1-y}$ $(x=0.25,\ y=0.55)$. They are obtained from Eq. (6) (3D M_0) for the $E_0/(E_0+\Delta_0)$ gap contribution, from Eq. (18) with $\Gamma=0.11$ eV (2D M_0) for the $E_1/(E_1+\Delta_1)$ gap contribution, and from Eq. (21) (DHO) for the E_0' (E_2) gap contribution. The sum of these contributions [including $\epsilon_{1\infty}$ $(=2.1)$] is also shown by the bold line. The calculated results of Eq. (18) with $\Gamma=0$ eV are also drawn by the dashed lines.

for the $E_1/(E_1+\Delta_1)$ gap contribution, from Eq. (20) (DHO) for the E_0' (E_2) gap contribution, and from Eq. (27) for the E_g^L gap contribution. The sum of these contributions is shown by the bold line.

The transitions at the 3D M_0 edges $[E_0/(E_0+\Delta_0)]$ yield a continuous absorption obeying the well-known $\frac{1}{2}$ power law [i.e., $(\hbar\omega-E_0)^{0.5}$]. The transitions at the E_g^L gap provide a gradually increasing absorption spectrum characterized by a power law of $(\hbar\omega-E_g^L)^2$. The steep high-energy end of the E_g^L gap contribution at the E_1 edge is the result of the E_c cutoff energy modification. The $E_g^{\rm id}$ transitions may also occur at energies above E_c $(=E_1)$. However, the ensuing $E_1/(E_1+\Delta_1)$ and E_0' (E_2) transitions can provide sufficient strengths, and thus take over the $E_g^{\rm id}$ gap oscillators present at above E_c. The $E_1/(E_1+\Delta_1)$ gaps are of the 3D M_1 (or 2D M_0) type, and hence the line shape of the corresponding ϵ_2 spectrum should be characterized by a steep low-energy side and a broader high-energy side. This line shape is in good agreement with the experimental verification. The E_0' (E_2) structure can be well characterized by the DHO model [Eq. (20)]. It has already been pointed out[18] that the DHO is a different representation of a broadened 2D M_1 CP.

In Fig. 9 we show an individual contribution to ϵ_1 of the $E_0/(E_0+\Delta_0)$, $E_1/(E_1+\Delta_1)$, and E_0' (E_2) transitions for $In_{1-x}Ga_xAs_yP_{1-y}$ $(x=0.25,\ y=0.55)$. They are obtained from Eq. (6) (3D M_0) for the $E_0/(E_0+\Delta_0)$ gap contribution, from Eq. (18) with $\Gamma=0.11$ eV (2D M_0) for the $E_1/(E_1+\Delta_1)$ gap contribution, and from Eq. (21) (DHO) for the E_0' (E_2) gap contribution. The sum of these contributions [including $\epsilon_{1\infty}$ $(=2.1)$] is also shown by the bold line. The calculated results of Eq. (18) with $\Gamma=0$ eV are also shown—by the dashed lines.

It is easily recognized from Fig. 9 that the $E_0/(E_0+\Delta_0)$ transitions strongly contribute to the dispersion of ϵ_1, but not to its absolute value. It is also clear that the strong negative peak observed in the E_0' (E_2) structure region is well explained by the DHO model (broadened 2D M_1 model). The CP structure of the E_0' (E_2) gap in InP has been explained by a mixture of a 3D M_0 and a 3D M_1 line shape.[8] However, we find here that neither the 3D M_0 nor the 3D M_1 model explain the peculiar line shapes of both ϵ_2 and ϵ_1 which appeared in the E_0' (E_2) spectral region of $In_{1-x}Ga_xAs_yP_{1-y}$ alloys. We can, therefore, consider that the best representation of the E_0' (E_2) structure is the DHO (i.e., broadened 2D M_1).

B. Strength parameters as a function of alloy composition

The strength of the $E_0/(E_0+\Delta_0)$ transitions is represented by A [see Eqs. (5) and (6)]. These transitions strongly contribute to the dispersion of $\epsilon_1(\omega)$, but not to its absolute value (see Fig. 9). Spectroscopic-ellipsometry work by Kelso *et al.*[8] was limited to the photon-energy range 1.5–6.0 eV. As recognized in Eq. (3), however, the E_0 gap energies of the $In_{1-x}Ga_xAs_yP_{1-y}$ alloys were much smaller than 1.5 eV. Therefore we were not able to see any distinctive structure of the E_0 transitions in the ϵ_2 spectra of Kelso's data; in other words, Kelso's experimental data are not sufficient for discussing the $E_0/(E_0+\Delta_0)$ strength. Because of this, we have tried to obtain the strength of A by fitting our model [Eq. (5)] with the optical-absorption data of $In_{1-x}Ga_xAs_yP_{1-y}$ $(y=0,\ 0.25,\ 0.64,$ and $1.0)$ (Ref. 30). The values of A as a function of alloy composition y for $In_{1-x}Ga_xAs_yP_{1-y}$, determined by this fitting, are shown in Fig. 10. The plots suggest that the value of A varies almost linearly with the alloy composition y. From the figure, we obtain the following relation (solid line):

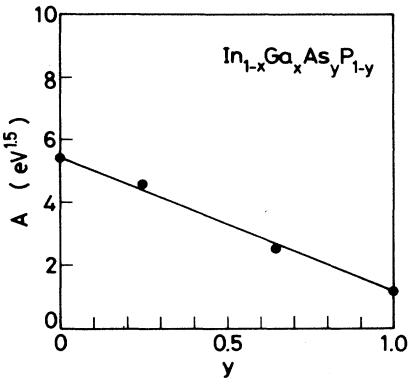

FIG. 10. The strength parameter A [$E_0/(E_0+\Delta_0)$ transitions] as a function of alloy composition y for $In_{1-x}Ga_xAs_yP_{1-y}$.

$$A(y)=5.4-4.2y \ . \tag{29}$$

The contribution to the dielectric susceptibility arises predominantly from the $E_1/(E_1+\Delta_1)$ transitions. The strength of the $E_1/(E_1+\Delta_1)$ transitions is represented by B's [see Eqs. (13)–(18)]. In Fig. 11 we show the variation of B_1 and B_2 (solid circles) as a function of alloy composition y for $In_{1-x}Ga_xAs_yP_{1-y}$. These plots suggest that both B_1 and B_2 vary in the quadratic forms (solid lines):

$$B_1(y)=4.91-3.85y+2.78y^2 \ , \tag{30a}$$

$$B_2(y)=0.09+2.65y-1.26y^2 \ . \tag{30b}$$

The strength of the $E_1/(E_1+\Delta_1)$ transitions of diamond-type (zinc-blende-type) materials can be theoretically estimated with the simple expressions

$$B_1=44\frac{E_1+(\Delta_1/3)}{a_0E_1^2} \ , \tag{31a}$$

$$B_2=44\frac{E_1+(2\Delta_1/3)}{a_0(E_1+\Delta_1)^2} \ , \tag{31b}$$

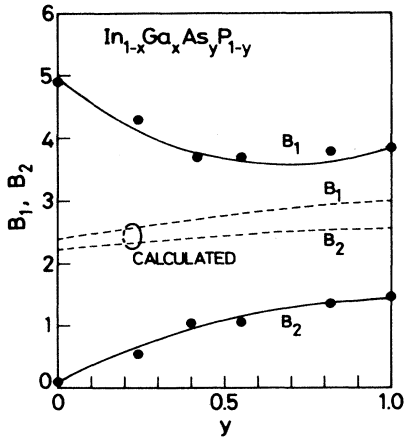

FIG. 11. The strength parameters B_1 and B_2 [$E_1/(E_1+\Delta_1)$ transitions] as a function of alloy composition y for $In_{1-x}Ga_xAs_yP_{1-y}$. The dashed lines are the calculated results of Eq. (31).

where a_0 is the lattice constant in Å and E_1 and Δ_1 are in eV. The dashed lines in Fig. 11 are the calculated results of these expressions. These calculated results indicate that B_1 and B_2 do not differ so largely with each other in a full range of the y composition. However, the experimental strength B_2 relative to B_1 increases dramatically with increasing y. This large difference in the experimental strengths was discussed in Ref. 8 and successfully explained in terms of the k-linear interaction (also see Refs. 31–34).

The variation of B_{11} as a function of alloy composition y for $In_{1-x}Ga_xAs_yP_{1-y}$ is shown in Fig. 12. The solid line represents fit of the data to the quadratic equation

$$B_{11}(y)=10.32-8.93y+6.18y^2 \ . \tag{32}$$

From the present and the previous works (Refs. 17–20), we are also able to find an empirical relation between B_1 and B_{11} (B_2 and B_{21}): $B_1\approx B_{11}/2$ ($B_2\approx B_{21}/2$) (see Table III).

In Fig. 13 we show the variation of $\Gamma(E_1/(E_1+\Delta_1))$ as a function of alloy composition y for $In_{1-x}Ga_xAs_yP_{1-y}$. The figure clearly suggests that Γ varies in the quadratic form,

$$\Gamma(y)=0.14-0.10y+0.10y^2 \ . \tag{33}$$

The damping effect should, in general, be influenced not only by temperature (i.e., *the thermal broadening through emission and absorption of phonons*), but also by potential fluctuations resulting from random atomic placement in the alloy (i.e., *the alloy disorder*). The thermal broadening ensures that the lower the temperature, the smaller the Γ value. If we assume that the degree of alloy disorder is proportional to $x(1-x)+y(1-y)$, it becomes maximum at $y=0.60$ for $In_{1-x}Ga_xAs_yP_{1-y}$. One can therefore expect that the value of Γ increases with y, showing a *maximum* for $y\approx 0.6$, then decreases with further increase of y. Such a simple consideration interpreted disorder-related effects well, e.g., on the lattice thermal conductivity in this material.[26] However, for the present case, Γ decreased with

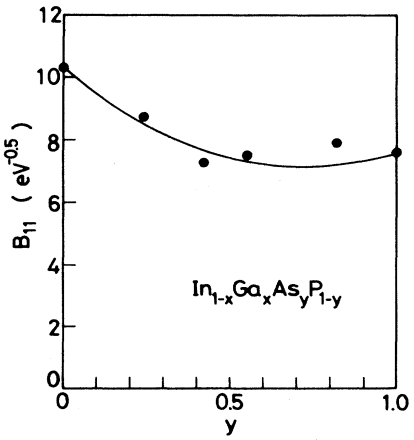

FIG. 12. The strength parameter B_{11} (E_1 transitions) as a function of alloy composition y for $In_{1-x}Ga_xAs_yP_{1-y}$.

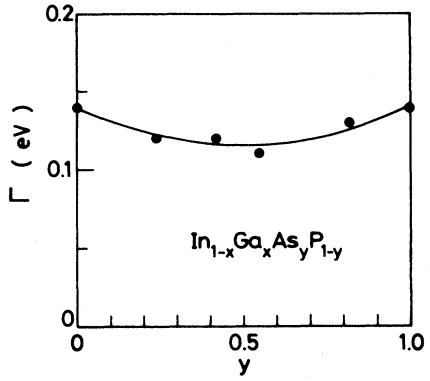

FIG. 13. The broadening factor Γ [$E_1/(E_1+\Delta_1)$ transitions] as a function of alloy composition y for $In_{1-x}Ga_xAs_yP_{1-y}$.

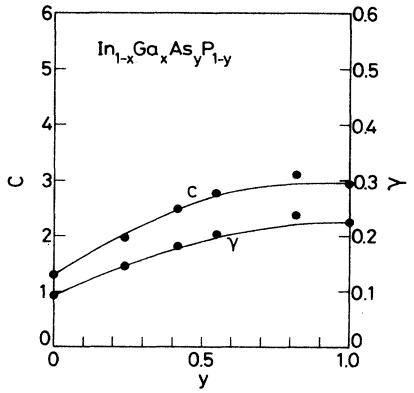

FIG. 14. The strength parameter C and broadening factor γ [E_0' (E_2) transitions] as a function of alloy composition y for $In_{1-x}Ga_xAs_yP_{1-y}$.

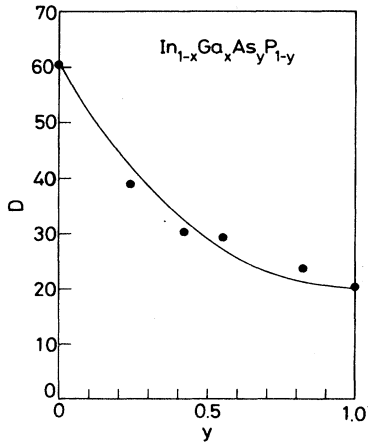

FIG. 15. The strength parameter D (indirect-band-gap transitions) as a function of alloy composition y for $In_{1-x}Ga_xAs_yP_{1-y}$.

y to a *minimum* value of 0.11 eV for $y=0.55$, then increased to 0.14 eV for $y=1.0$. This is a direct contrast to that expected from the simple consideration above. One should also note that some crystalline-imperfection effects, e.g., crystal qualities, may affect the dielectric susceptibility. Unfortunately, however, at present we do not make clear the origin of the observed variation in $\Gamma(E_1/(E_1+\Delta_1))$.

The strength of the E_0' (E_2) transitions is represented by C [see Eqs. (20) and (21)]. The variation of C and γ (damping parameter) as a function of alloy composition y for $In_{1-x}Ga_xAs_yP_{1-y}$ is shown in Fig. 14. Like the B's and Γ, the variation of C and γ can be fitted by the quadratic equations

$$C(y)=1.30+3.70y-2.10y^2\ , \tag{34a}$$

$$\gamma(y)=0.093+0.256y-0.124y^2\ . \tag{34b}$$

The results of these fits are shown by the solid lines in the figure.

The strength of the E_g^{id} (indirect-band-gap) transitions can be represented by D [see Eq. (27)]. We show in Fig. 15 the variation of D as a function of alloy composition y for $In_{1-x}Ga_xAs_yP_{1-y}$. The solid line represents fits of the data to the quadratic equation

$$D(y)=60.4-83.9y+44.2y^2\ . \tag{35}$$

As mentioned in Sec. II, the dielectric function is expressed by the band-structure parameters (band-gap energies) and the corresponding strength and broadening parameters. In this section we have specified these parameters in terms of y alone. By applying these results, therefore, we can easily calculate the spectral dependence of the dielectric constants [$\epsilon_1(\omega)$ and $\epsilon_2(\omega)$] for optional composition of $In_{1-x}Ga_xAs_yP_{1-y}$ lattice matched to InP.

IV. CONCLUSIONS

We have developed a method for calculation of the real (ϵ_1) and imaginary (ϵ_2) parts of the dielectric function of $In_{1-x}Ga_xAs_yP_{1-y}$ quaternaries lattice matched to InP ($0\le y\le 1.0$) at energies below and above the fundamental absorption edge. The model is based on the Kramers-Kronig transformation and takes into account the effects of optical transitions at the E_0, $E_0+\Delta_0$, E_1, $E_1+\Delta_1$, and E_0' (E_2) CP's and indirect band gap (E_g^{id}). This model reveals distinct structures at energies of the E_0 and $E_0+\Delta_0$ (3D M_0 CP's), E_1 and $E_1+\Delta_1$ (3D M_1 or 2D M_0 CP's), and E_0' (E_2) [DHO (broadened 2D M_1)]. The E_g^{id} transitions are assumed to yield a continuous $\epsilon_2(\omega)$ spectrum obeying the well-known square power law [i.e., $\propto(\hbar\omega-E_g^{id})^2$]. The calculated results are in satisfactory agreement with the experimental data over the entire range of photon energies (0–6.0 eV). The compositional dependence of the optical-transition strength and broadening parameters at energies of each CP and in-

direct band gap is also obtained and discussed. The dielectric function of $In_{1-x}Ga_xAs_yP_{1-y}$ can then be specified in terms of y alone. This ensures that one can easily calculate the spectral dependence of the dielectric function for optional composition of $In_{1-x}Ga_xAs_yP_{1-y}$. Dielectric-connected optical constants, such as the refractive indices and absorption coefficients, are also easy to obtain from the present study in the form of practical functions.

ACKNOWLEDGMENTS

This work was supported in part by the Gunma University Foundation for Science and Technology, Gunma, Japan.

[1]See, for example, *Semiconductors and Semimetals,* edited by W. T. Tsang (Academic, New York, 1985), Vol. 22, Pts. A–D.
[2]J. Friedel, G. Harbeke, F. Abéles, B. O. Seraphin, J. Tauc, V. Spicer, J. Ducuing, and C. Flytzanis, in *Optical Properties of Solids,* edited by F. Abéles (North-Holland, Amsterdam, 1972).
[3]D. E. Aspnes, in *Optical Properties of Solids, New Developments,* edited by B. O. Seraphin (North-Holland, Amsterdam, 1976).
[4]D. E. Aspnes and A. A. Studna, Phys. Rev. B **27**, 985 (1983).
[5]P. Lautenschlager, M. Garriga, L. Viña, and M. Cardona, Phys. Rev. B **36**, 4821 (1987).
[6]L. Viña, S. Logothetidis, and M. Cardona, Phys. Rev. B **30**, 1979 (1984).
[7]L. Viña, H. Höchst, and M. Cardona, Phys. Rev. B **31**, 958 (1985).
[8]S. M. Kelso, D. E. Aspnes, M. A. Pollack, and R. E. Nahory, Phys. Rev. B **26**, 6669 (1982).
[9]S. Logothetidis, L. Viña, and M. Cardona, Phys. Rev. B **31**, 947 (1985).
[10]M. Erman, J. P. Andre, and J. LeBris, J. Appl. Phys. **59**, 2019 (1986).
[11]D. E. Aspnes, S. M. Kelso, R. A. Logan, and R. Bhat, J. Appl. Phys. **60**, 754 (1986).
[12]M. Garriga, P. Lautenschlager, M. Cardona, and K. Ploog, Solid State Commun. **61**, 157 (1987).
[13]P. Lautenschlager, M. Garriga, S. Logothetidis, and M. Cardona, Phys. Rev. B **35**, 9174 (1987).
[14]P. Lautenschlager, M. Garriga, and M. Cardona, Phys. Rev. B **36**, 4813 (1987).
[15]S. Logothetidis, M. Cardona, P. Lautenschlager, and M. Garriga, Phys. Rev. B **34**, 2458 (1986).
[16]L. Viña, C. Umbach, M. Cardona, and L. Vodopyanov, Phys. Rev. B **29**, 6752 (1984).
[17]S. Adachi, Phys. Rev. B **35**, 7454 (1987).
[18]S. Adachi, Phys. Rev. B **38**, 12 345 (1988).
[19]S. Adachi, Phys. Rev. B **38**, 12 966 (1988).
[20]S. Adachi, J. Appl. Phys. (to be published).
[21]R. E. Nahory, M. A. Pollack, W. D. Johnston, Jr., and R. L. Barns, Appl. Phys. Lett. **33**, 659 (1978).
[22]E. H. Perea, E. E. Mendez, and C. G. Fonstad, Appl. Phys. Lett. **36**, 978 (1980).
[23]J. R. Chelikowsky and M. L. Cohen, Phys. Rev. B **14**, 556 (1976).
[24]M. Cardona, K. L. Shaklee, and F. H. Pollak, Phys. Rev. **154**, 696 (1967).
[25]S. Adachi, J. Appl. Phys. **53**, 5863 (1982).
[26]S. Adachi, J. Appl. Phys. **54**, 1844 (1983).
[27]S. Adachi, J. Appl. Phys. **53**, 8775 (1982); **54**, 6620 (1983); **56**, 74 (1984); **56**, 1499 (1984); **61**, 4869 (1987).
[28]S. Adachi, J. Appl. Phys. **58**, R1 (1985).
[29]In obtaining this equation, the following lattice constants (a_0's) were used: for GaP $a_0=5.4512$ Å, for GaAs $a_0=5.6533$ Å, for InP $a_0=5.8688$ Å, and for InAs $a_0=6.0584$ Å.
[30]W. Kowalsky, H.-H. Wehmann, F. Fiedler, and A. Schlachetzki, Phys. Status Solidi A **77**, K75 (1983), and references therein.
[31]E. O. Kane, Phys. Rev. **175**, 1039 (1968).
[32]M. Cardona, Phys. Rev. B **15**, 5999 (1977).
[33]D. E. Aspnes and M. Cardona, Solid State Commun. **27**, 397 (1978).
[34]A. Daunois and D. E. Aspnes, Phys. Rev. B **18**, 1824 (1978).